Proceedings of the 28th IEEE
EMBS Annual International Conference
New York City, USA, Aug 30-Sept 3, 2006

A Fast Linear Reconstruction Method for Scanning Impedance Imaging

Hongze Liu, Aaron R. Hawkins, Stephen M. Schultz, and Travis E. Oliphant
Department of Electrical and Computer Engineering, Brigham Young University, UT, USA

***Abstract*— Scanning electrical impedance imaging (SII) has been developed and implemented as a novel high resolution imaging modality with the potential of imaging the electrical properties of biological tissues. In this paper, a fast linear model is derived and applied to the impedance image reconstruction of scanning impedance imaging. With the help of both the deblurring concept and the reciprocity principle, this new approach leads to a calibrated approximation of the exact impedance distribution rather than a relative one from the original simplified linear method. Additionally, the method shows much less computational cost than the more straightforward nonlinear inverse method based on the forward model. The kernel function of this new approach is described and compared to the kernel of the simplified linear method. Two-dimensional impedance images of a flower petal and cancer cells are reconstructed using this method. The images reveal details not present in the measured images.**

I. Introduction

A device that allows the scientist to explore the details of the electrical properties of a cell or a group of cells could be beneficial to understanding cell anatomy and function, and assist in the treatment of various diseases, especially cancers[1], [2], [3], [4], [5]. The previously presented scanning impedance imaging (SII) system seeks to produce micron-scale images of the electrical properties of small tissues by measuring electrical impedance[6], [7]. Due to the unique configuration of indirect contact and high-resolution scanning techniques, SII has shown the potential to provide microscopic images of small tissues *in vitro* with the help of a shielded-probe design. Thus, SII has many potential applications in biology, such as tissue analysis or the *in vitro* monitoring and imaging of a single cell.

The detailed design and implementation of the SII system were presented elsewhere[6] and is only reviewed here. A typical SII system consists of two primitive components as illustrated in Fig. 1: an impedance probe suspended above a sample on a conducting plane, and a conducting solution surrounding the sample and the probe providing an electrical path between them. A two-dimensional image can be obtained by taking measurements at different horizontal positions. Usually, a coaxial shielded probe is used, which has a central core of metal surrounded by a non-conducting medium enclosed by a cylindrical metal shielding.

The physical theory behind the SII system can be derived from Maxwell's equations (specifically Gauss's law and continuity of charge) and Ohm's law[8]. The fundamental formulation is

$$\bigtriangledown \cdot (\sigma \bigtriangledown \phi) = 0, \tag{1}$$

where σ is the conductivity and ϕ is the potential inside the conducting region. The measured current I is related to ϕ as,

$$I = \int_S \sigma \bigtriangledown \phi \cdot \hat{n} ds, \tag{2}$$

where the surface S (oriented with normal $\hat{n}$) is the end of the tip. Because ϕ is a non-linear function of σ, it can be seen that the image reconstruction of σ from the measurements of I is a complicated inverse problem. This entire problem can be solved by a regularized parameter identification algorithm. This algorithm must be initialized with a first guess of the impedance distribution, usually taken as uniform. Next, a computer model simulates the measuring process. By comparing the simulated currents to the data, we update the impedance estimation until they agree. It can be noticed that in each iteration, the simulation of the measuring process requires solving (1) at each scanning position. Thus, this algorithm results in a huge computational cost which is not applicable for a quick image reconstruction.

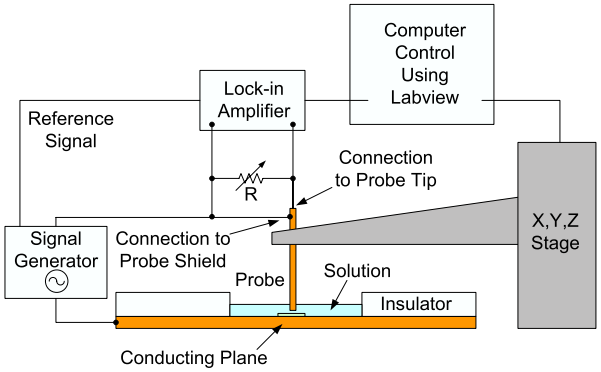

Fig. 1. Diagram of a typical SII system.

In this paper, we develop a fast linear approach based on the deblurring concept and the reciprocity principle[9] for the image reconstruction of SII system. This method is much faster than the more traditional iterative solution mentioned above and can achieve a calibrated reconstructed image that approximately describes the real conductivity distribution.

II. Reconstruction Methods

A. Reciprocity principle linear reconstruction (RPL)

1) Reciprocity principle: Consider the region of interest in an SII system as a conducting domain Ω with conductivity σ as illustrated in Fig. 2. A voltage U_1^t is applied to the tip while another voltage U_1^s drives the shield, which leads to an electric scalar potential distribution ϕ_1 due to the

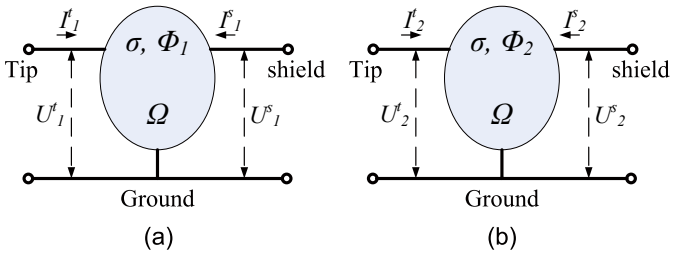

Fig. 2. Conducting region Ω with conductivity σ. (a) A voltage U_1^t applied to the tip and another voltage U_1^s applied to the shield lead to a potential distribution ϕ_1. The current through the tip I_1^t and the current through the shield I_1^s can be measured. (b) Changing the voltage on the shield to zero results in a different potential distribution ϕ_2 with different currents I_2^t, I_2^s.

conductivity of the region. Hence, a current through the tip I_1^t and a current through the shield I_1^s can be measured. Then, if we connect the shield to the ground ($U^s = 0$), the potential distribution ϕ_2 will be different from the distribution of case A. This results in different values of I_2^t through the tip and I_2^s through the shield.

For the first case, Ohm's law is

$$J_1 = -\sigma \bigtriangledown \phi_1, \tag{3}$$

where J_1 is the current density in the domain Ω. Multiply the voltage obtained in the second case, ϕ_2, on both sides and integrate the equation over the boundary $\partial\Omega$:

$$\int_{\partial\Omega} J_1\phi_2 \cdot ds = -\int_{\partial\Omega} \phi_2\sigma \bigtriangledown \phi_1 \cdot ds. \tag{4}$$

The normal component of J_1 is zero everywhere on the boundary except for on the conducting plane, the tip and the shield. The voltage, ϕ_2 is zero on the conducting plane and on the shield. The voltage on the tip for the second case is U_2^t and the current through the tip in the first case is I_1^t. Thus, the left-hand side of the previous equation simplifies to $U_2^t I_1^t$. Applying Gauss' theorem to the right-hand side, we can rewrite (4) as

$$U_2^t I_1^t = -\int_\Omega \bigtriangledown \cdot (\phi_2\sigma \bigtriangledown \phi_1)\, d\Omega. \tag{5}$$

To simplify the right-hand side, notice that

$$\bigtriangledown \cdot (\phi_2\sigma \bigtriangledown \phi_1) = \sigma \bigtriangledown \phi_2 \cdot \bigtriangledown\phi_1 + \phi_2 \bigtriangledown \cdot (\sigma \bigtriangledown \phi_1), \tag{6}$$

and because$\bigtriangledown\cdot(\sigma \bigtriangledown \phi_1) = 0$ for all the points in the domain, (5) simplifies to

$$I_1^t = -\frac{1}{U_2^t}\int_\Omega \sigma \bigtriangledown \phi_2 \cdot \bigtriangledown\phi_1 d\Omega. \tag{7}$$

This equation establishes an explicit relationship between the current through the tip and the conductivity distribution in the region Ω. The ϕ_2 and ϕ_1 voltage distributions are themselves dependent on σ. But, for small changes in conductivity it may be possible to approximate ϕ_2 and ϕ_1 using an average value of conductivity so that the relationship between I_1^t and conductivity is linear. In addition, far from the boundaries of the sample, the linear operator can be considered shift-invariant (at least in two-dimensions). When the linear and shift-invariant approximations are valid, deconvolution can be used to reconstruct images of conductivity.

2) Deconvolution: In (7), it can be seen that if we assume both shift-invariance and that ϕ_2 and ϕ_1 are not functions of σ. Then, the current is a convolution of the conductivity distribution with some kernel function.

$$I(\mathbf{x}') = \int \sigma(\mathbf{x}) K(\mathbf{x}' - \mathbf{x})\, d\mathbf{x}, \tag{8}$$

where

$$K(\mathbf{x}) = -\frac{1}{U}\nabla\phi_2(-\mathbf{x}) \cdot \nabla\phi_1(-\mathbf{x}). \tag{9}$$

Our SII system only takes 2-D data, and it is more difficult to justify shift-invariance in the third dimension. Thus, the linear equation more appropriate for SII is

$$I(x, y) = \sigma(x, y) \star k(x, y) \tag{10}$$

where $\sigma(x, y) = \int \sigma(\mathbf{x})\, dz$ and

$$k(x, y) = \frac{\int dz\sigma(\mathbf{x}) K(\mathbf{x})}{\int dz\sigma(\mathbf{x})}. \tag{11}$$

To reconstruct the conductivity distribution, we can implement the deconvolution using a Fourier transform,

$$\hat{I} = \hat{\sigma}\hat{k}, \tag{12}$$

$$\hat{\sigma}_\alpha = \frac{\hat{k}^*\hat{I}}{\left\{|\hat{k}|^2 + \alpha\right\}}. \tag{13}$$

It can be seen that in the RPL method, (1) only needs to be solved once for one configuration. This results in a much faster reconstruction compared to the implicit inverse method.

B. Simplified linear reconstruction (SL)

Previously, an even simpler linear analysis was conducted which additionally used the method of images to derive the voltage for the case of homogeneous background conductivity. To compare to the RPL method, the original simplified linear method is reviewed here. Consider the current I through a tip placed a distance h above the conducting ground plane. In a small region, we assume that the electric field does not differ significantly from the one in a homogeneous material. Assuming shift invariance, we can then obtain a thin-sample, two-dimensional, simplified, linear, shift-invariant model[10]:

$$I = \frac{cq}{2\pi\epsilon h^2} K_h \star \sigma, \tag{14}$$

where q is the charge on the idealized, infinitesimal tip, c is a proportionality constant due to the shield, and K_h is

$$K_h(x, y) = \frac{h^3}{(x^2 + y^2 + h^2)^{3/2}}. \tag{15}$$

Unlike the RPL method, we cannot obtain the exact value of σ from I, since the coefficient $\frac{qc}{2\pi\epsilon h^2}$ cannot be determined without experiment. Thus, the SL method is most suitable for producing a relative image of σ. On the other hand, the RPL method provides a calibrated way to estimate the exact value of σ.

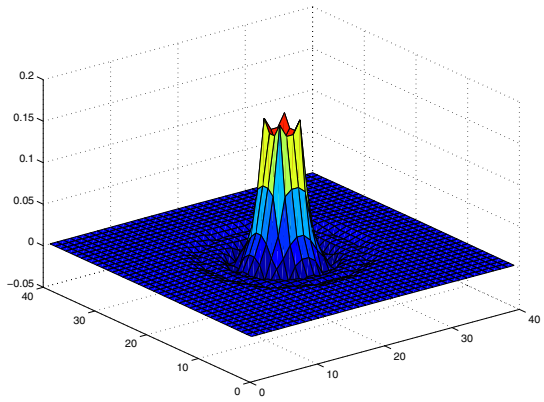

(a)

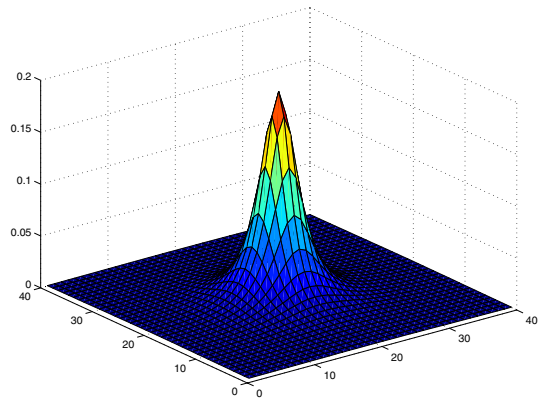

(b)

Fig. 3. The shaded surface plot of two-dimensional kernel function. (a) the RPL method, (b) the SL method.

III. Kernel function

In our SII system, we can obtain a current map at a particular distance above the sample. As shown in (7), this current map is a blurred image of the exact impedance distribution of the sample. In order to reconstruct the impedance image, one important task of the RPL method is to calculate the kernel function in (9) for the SII system. The key part of this kernel function is the determination of ϕ. For a given σ, ϕ can be solved from (1) plus boundary conditions. Here we use a finite difference method (FDM) to solve this partial differential equation. To simplify the computation of this approach, we assume that σ is homogeneous in the region of interest with an average value of the simple impedance image σ_s , which is defined as

$$\sigma_s = \frac{U}{I_m}. \tag{16}$$

where I_m is the measured current map and U is the voltage of the tip.

Fig. 3(a) shows the shaded surface plot of a two-dimensional kernel function obtained using this approach. The tip diameter and the shield thickness are both 30 μm while the gap spacing between the shield and the tip is also 30 μm wide. The potential ϕ_1 is simulated using FDM with a

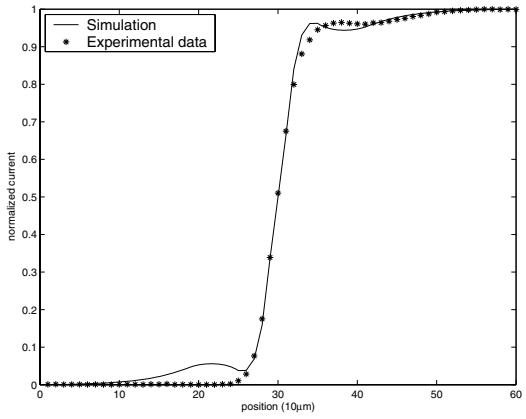

Fig. 4. Measured results of a line scan using a (30μm tip diameter, 30μm gap spacing, 30μm shield thickness) shielded probe and a 170-μm thick glass slice for an insulator along with the simulated result using the RPL method under same conditions.

2.3V voltage applied to the tip and a 2.5V voltage applied to the shield. Then, we obtain ϕ_2 by repeating the same process except using zero voltage on the shield. For comparison, a kernel function of the SL method is also obtained with $h = 35\mu$m as illustrated in Fig. 3(b). It can be observed that the kernel function of the RPL method has a sharper edge and represents more details of the probe structure than the SL method kernel. The sharper edge shows that the RPL method might be able to reveal the shield function better than the SL method since the shield helps to shrink the average cross-section area of current flow through the sample.

IV. Results and analyses

To experimentally verify the method, a line-scanning experiment was performed using the SII system. A line-scan is defined as a line profile scanned across an abrupt change in impedance such as from the insulator to the conducting plane in one horizontal direction. In the experiment, a 170-μm thick glass slice was immersed in an aqueous solution (water with resistivity of 10 kΩ-cm) on a conducting (aluminum wafer) plane. A shielded probe (30μm tip diameter, 30μm gap spacing, 30μm shield thickness) was suspended at a 25-μm distance above the glass. A Newmark System Model NLS4-4-16 XYZ was used as a stage controller to move the probe for scanning horizontally at increments down to 10μm. A 2.5 Volt peak to peak, 10kHz AC signal generated by a programmable frequency generators (Agilent 3520A) was applied to the shield directly and drove the tip through a 27kΩ resistor. A DSP lock-in amplifier (EG&G Instruments Model 7265) collected the voltage across the resistor, which is proportional to the current through the tip.

Fig. 4 shows the experimental data along with the simulated line profile using the RPL method under same conditions. In the simulation, we created an impedance distribution that is the same as the one used in the experiment. Then, we obtained the current map by calculating the convolution in (10). The line profile is one line in the simulated current map along the scanning direction. Both curves are linearly

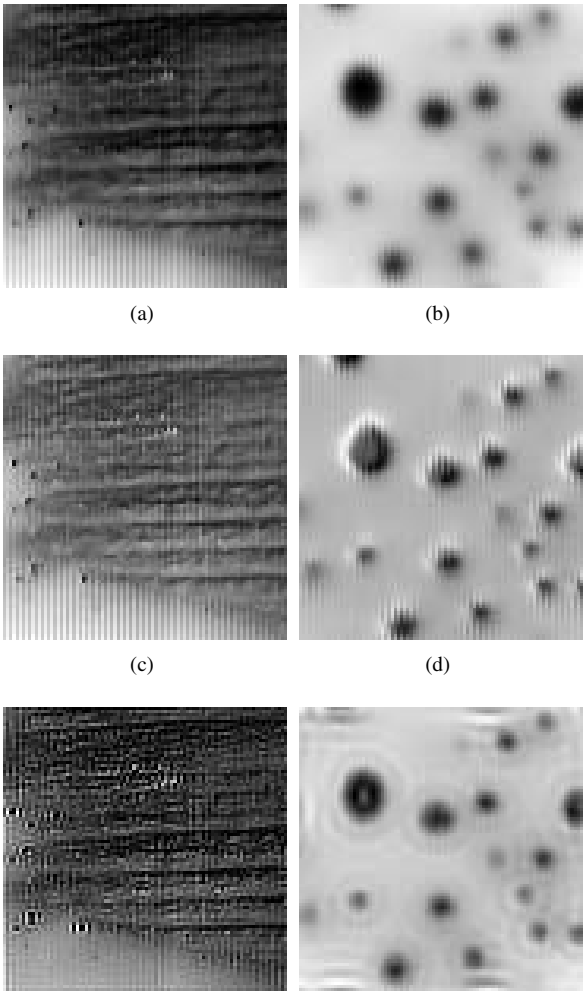

Fig. 5. (a), (c),(e) a purple flower petal, pixel size 25.4μm$\times$25.4μm, image size 2.29mm$\times$2.29mm; (b), (d), (f) breast cancer cell groups, pixel size 10μm$\times$10μm, image size 0.9mm$\times$0.9mm. (a), (b) are the measured current map; (c), (d) are the reconstructed images using the SL method; (e), (f) are reconstructed images using the RPL method.

scaled to lie between 0 and 1. Validation of the RPL method is evident in the reasonable fit between the two curves. Differences can be observed at the beginning and the end of the slope. One possible explanation is that ϕ is calculated under the homogeneous assumption of local impedance which is not necessarily a good approximation due to the abrupt impedance change in this case. Thus, this data-fitting exercise can be considered a worse-case scenario. If conductivity changes are less abrupt we can expect the simplified model to work better.

To demonstrate image reconstruction using the linearized approximation, two images of small tissues were collected and reconstructed. Fig. 5 shows the experimental data, the reconstructed images of the SL method and the results reconstructed using the RPL method for a purple flower petal and breast cancer cell groups. The experimental data of the cancer cells were generated under same condition as the line scan while the data of the flower petal were produced with a (100-μm tip diameter) probe scanned at a 25-μm step size. It can be observed that both methods can help to improve the resolution and reveal the details not present in the measured images. Further, the RPL method can pick up high frequency components as shown in Fig. 5 (e) and (f). One possible explanation is that it takes into account both the geometry of the probe and the function of the shield in its kernel.

V. Conclusion

In this paper, we applied the reciprocity principle to our SII system to obtain a linear approximation to the non-linear relationship between current and conductivity. The method and its kernel function have been compared to the simplified linear approach that was presented earlier. Method verification has been achieved by comparing the simulated line-scanning result with experimental data under same conditions with a known conductivity distribution. Good correspondence has shown this method can describe the SII system reasonably well. Two-dimensional images of a flower petal and cells were also obtained using the SII system and reconstructed using both the RPL method and the SL method. The results indicated that both methods can help improve the resolution. The RPL method can provide a calibrated image of the conductivity distribution. Also, the computation cost and the programming effort of the RPL method are both much less than those of the numerical nonlinear inverse method based on a true forward model.

References

[1] F. C. Grant. Localisation of brain tumours by determination of the electrical resistance of the growth. *Journal of the American Medical Association*, 81:2166–2169, 1923.

[2] G. J. Saulnier, R. S. Blue, J. C. Newell, D. Isaacson, and P. M. Edic. Electrical impedance tomography. *IEEE Signal Processing Magazine*, pages 31–43, November 2001.

[3] A. Malich, T. Fritsch, R. Anderson, T. Boehm, M.G. Freesmeyer, M. Fleck, and W.A. Kaiser. Electrical impedance scanning for classifying suspicious breast lesions: first results. *European Radiology*, 10(10):1555–1561, September 2000.

[4] V. A. Cherepenin, A. Y. Karpov, A. V. Korjenevsky, V. N. Komienko, Y. S. Kultiasov, M. B. Ochapkin, O. V. Trochanova, and J. D. Meister. Three-dimensional eit imaging of breast tissues: System design and clinical testing. *IEEE Transactions on Medical Imaging*, 21(6):662–667, June 2002.

[5] R. Shao, S. V. Kalinin, and D. A. Bonnell. Local impedance imaging using spectroscopy of polycrystalline zno using contact atomic force microscopy. *Applied Physics Letters*, 82(12):1869–1871, March 2003.

[6] Aaron R. Hawkins, Hongze Liu, Travis E. Oliphant, and Stephen M. Shultz. Non-contact scanning impedance imaging in an aqueous solution. *Applied Physics Letters*, 85(5), August 2004.

[7] Benjamin C. Green, Tao Shang, Jacey C. Morine, Hongze Liu, Stephen M. Schultz, Travis E. Oliphant, and Aaron R. Hawkins. Resolution scaling in noncontact scanning impedance imaging. *Review of Scientific Instruments*, 2005.

[8] J.D. Jackson. *Clasical Electrodynamics*. John Wiley and Sons, New York, second edition, 1975. Chapter 2.

[9] Bernhard Brandstatter. Jacobian calculation for electrical impedance tomography based on the reciprocity principle. *Ieee Transactions on Magnetics*, 39(3), May 2003.

[10] Travis E. Oliphant, Hongze Liu, Tao Shang, Stephen M. Schultz, and Aaron R. Hawkins. Scanning impedance imaging of biological samples. *IEEE Transactions on Biomedical Engineering*, 2006.